# Measuring transverse beam emittance using a 2.07 GHz movable Schottky cavity at the Relativistic Heavy Ion Collider

K. A. Brown,* M. Blaskiewicz, C. Degen, and A. Della Penna
*C-AD Department, BNL, Upton, New York 11973-5000, USA*
(Received 16 May 2008; published 13 January 2009)

Using a movable Schottky cavity resonant at 2.07 GHz, we have developed a simple method of deriving the beam sizes at the detector. In this report we will explain the theory behind the method, describe the system and the signal processing, and then present the results from experiments using this method. We will also present our plans for using this new technique for obtaining beam emittances during normal operation of the Relativistic Heavy Ion Collider (RHIC) at Brookhaven National Laboratory (BNL).

DOI: 10.1103/PhysRevSTAB.12.012801 PACS numbers: 41.85.Ew, 29.27.Fh

## I. INTRODUCTION

In particle accelerators and high energy colliders, there are various methods used to measure the beam size, from which we derive the beam emittance (a nice overview of the various methods is given by Koziol [1].) Most methods for measuring beam size are intrinsically destructive to the beam. Significant work is invested into minimizing the interaction of the beam with the instruments, although some devices are less destructive than others. In the Relativistic Heavy Ion Collider (RHIC) there are five systems that can directly measure beam size or from which the beam size can be derived.

One method for measuring beam size that is important for calibrating luminosity at RHIC is to perform a luminosity (or vernier) scan [2–4]. The beams are scanned across each other at the collision point and, using beam position measurements, the amount of motion is correlated with detectors monitoring the collisions. These scans are performed periodically but not for every RHIC cycle. From these scans a calibration is determined allowing the transverse beam emittances to be derived from measures of the luminosity and beam current. In vernier scans, however, the derived emittances are a convolution of the emittances of the two beams [5].

The beam sizes are also measured using four ionization profile monitors (IPM), one for each transverse plane for each of the two accelerators that comprise RHIC [6]. A high voltage accelerates electrons produced by the interaction of the beam with the residual gas to a set of electrodes that are outside of the beam region. In principle, such a system does not perturb the beam. In practice, at RHIC, the high voltage is pulsed, which perturbs the beam nonadiabatically. Therefore, to minimize emittance growth the frequency of sampling is reduced while beams are in collision. A significant advantage of using the IPMs is these instruments are capable of measuring single bunch and single turn beam sizes.

Another method used in RHIC is to derive beam size from scanning a thin carbon target across the beam [7]. The primary purpose of the carbon target is to monitor polarization during polarized proton operation. The targets consist of thin carbon ribbons ( $\sim 4\ \mu g/cm^2$) designed to minimally interact with the beam. Nevertheless, if left in the beam for too long, they will either break or increase the beam emittance noticeably. This system is also capable of measuring the single bunch and single turn beam sizes.

A fourth system that is currently being developed is to use a camera to measure the fluorescence induced by the passage of the beam through a hydrogen jet [8], which is primarily used to measure and calibrate the beam polarization in RHIC [9]. At present, this system is limited to measuring just the vertical beam size.

Each of the systems described above either perturbs the beam noticeably or has dependencies that make them difficult to calibrate. The purpose of developing a Schottky emittance monitor is to provide a simple nondestructive measurement during RHIC stores and to provide an alternative and backup system for monitoring emittance. As we will describe in this paper, the main advantage of this Schottky emittance monitor is the fact that it is completely a passive measurement, and does not cause emittance growth. Another significant advantage is that it is very simple to calibrate. The only part of the system that requires calibration are the translation stages used to move the cavity.

## II. OVERVIEW OF RHIC OPERATION

RHIC consists of two superconducting accelerators with counterrotating beams. It has six interaction regions where the two beams could be put into collisions with zero crossing angle. We currently operate with collisions in two of these regions. RHIC can be operated in many different modes and with many different types of beams [10]. For example, RHIC is able to run with two different ion beams in the two rings simultaneously (e.g., gold and deuteron beams in collision) [11]. RHIC can operate gold ions up to

*kbrown@bnl.gov

 

TABLE I. RHIC parameters from recent operation.

| Parameter | Recent value | Units |
|---|---|---|
| Circumference | 3833.845 | m |
| Revolution frequency ($v = c$) | 78.196 | kHz |
| Injection energy, gold | 10.38 | GeV/nucleon |
| Injection energy, protons | 23.8 | GeV |
| Store energy, gold | 100 | GeV/nucleon |
| Store energy, protons | 100 | GeV |
| Acceleration rf harmonic | 360 | |
| Number of bunches, gold | 103 | |
| Number of bunches, protons | 109 | |
| Number of collision points | 2 | |
| Intensity, gold | 1.1 | $10^9$ ions/bunch |
| Intensity, protons | 150 | $10^9$ protons/bunch |
| $\gamma_t$ | 22.89 | (lattice dependent) |
| Bunch length (rms) | 2.8 | nsec |

100 GeV/nucleon per ring and has achieved peak gold on gold luminosities of $30 \times 10^{26}$ cm$^{-2}$ sec$^{-1}$ [12]. RHIC is also capable of operating with polarized proton beams and has achieved peak luminosities of $35 \times 10^{30}$ cm$^{-2}$ sec$^{-1}$ [13]. As the beam intensities and luminosities are pushed higher, it becomes more and more desirable to have an alternative and nondestructive method of measuring emittance. Since RHIC is capable of running in so many different modes, the method needs to be robust and capable of working for different kinds of beams and beam intensities. Table I summarizes some basic parameters from recent RHIC operation. Note that these parameters change according to the configuration for a given operation. For example, $\gamma_t$ can change depending on the lattice choice. Betatron tunes [14] can be adjusted over a large range of values, but generally a working point is selected based on the beam dynamics and to achieve the longest beam lifetime during collisions [15]. RHIC fill patterns are adjusted according to the mode of running and other requirements. Timing constraints from the experiments require the rf buckets be filled modulo three (only every third bucket can have beam in it) and the abort kickers require a gap to exist in the bunch train to coincide with the rise time of the kickers. The bunch length given in the table is for the root-mean-square (rms) bunch length during RHIC store for polarized protons.

## III. INTRODUCTION TO SCHOTTKY SIGNALS

Schottky detectors exploit the statistical nature of the variations in the motion of the ensemble of particles in the accelerators. The theory describing the Schottky signal for particle beams is well described by van der Meer [16], Chattopadhyay [17], and Boussard [18]. Measuring the random variations in the motion of the ensemble of particles requires looking in the frequency domain, at high enough frequency to be well above the coherent signal. There are two modes in a Schottky detector that are of interest for beam diagnostics. One mode measures the longitudinal variations in the time of arrival of the particles. From this we can obtain the momentum spread from the distribution of frequencies and the beam current from the amount of power in the distribution. The other mode measures the transverse variations due to the betatron motion of the particles. From this we can obtain the betatron tune, from the average frequency in those variations, the chromaticity, from the difference in the width of the frequency distributions above and below the revolution line harmonic, and the beam size, reflected in the power in those frequencies.

There are a number of types of detectors that can be used to detect Schottky signals. Since these signals are extremely small, a significant amount of effort goes into the design of the detectors and processing of the signals. The detector we used is a high frequency cavity developed for RHIC by the Lawrence Berkeley National Laboratory Center for Beam Physics group when RHIC was being constructed. The properties of the cavity are well described by a report they published in 1998 [19]. The cavity uses four probes to detect signals from the different modes in the cavity. Two probes sample the transverse modes, at 2.067 and 2.071 GHz. They occur at different frequencies because the transverse dimensions of the device are different by about 0.5 mm. Two other probes sample the longitudinal mode which is at 2.742 GHz (one of these can be used to inject signals for calibration and testing). The cavity has a very high $Q_{\text{unloaded}} = 10\,000$ ($Q_{\text{loaded}}$ was measured to be approximately 4700 for normal operation [20]). The device has been available in RHIC for many years as a tune and chromaticity monitor.

For our purposes, what is important is to note that the signal sampled by the transverse mode probes will have three basic components in the frequency domain, at a given harmonic. As described above, there will be two distributions of spectral components (referred to as the betatron sidebands) equally spaced around the revolution harmonic. These sidebands contain the frequencies resulting from the betatron motion of the particles in the beam. The power in these sidebands is independent of the relative position of the device to the beam (in the central linear region of the device) and is proportional to the beam size. The third component is the distribution of frequencies around the revolution harmonic. The power in this component depends linearly on the relative position of the device to the beam.

## IV. THEORY

The total amount of power in the transverse modes can be calculated by noting that the signal measured by the transverse probes is a function of the relative position of the device to the beam. The dipole moment is given by

$$S(t) = I(t)X(t) = \sum_{k=1}^{N} \omega_k Q \delta_p(\omega_0 t + \phi_k(t)) \times \left[ X + \frac{(E_k - E_0)}{\beta^2 E_0} D + \hat{X}_k \cos(\omega_\beta t + \psi_k) \right], \quad (1)$$

where $\hat{X}_k$ corresponds to the single particle amplitude relative to the closed orbit, $E_k$ is the single particle energy, $\omega_\beta$ is the betatron frequency for that particle, $\omega_k$ is the angular revolution frequency for the particle, the particle charge is $Q$, and $\psi_k$ is the betatron phase. The position of the closed orbit relative to the electrical center of the cavity is $X$. The energy of the particle on the reference orbit is $E_0$, $\omega_0$ is the angular revolution frequency for that particle, $\beta = v/c$, where $v$ is the synchronous particle velocity, $D$ is the lattice momentum dispersion, $N$ is the number of particles, $t$ is time, and the periodic delta function is

$$\delta_p(\theta) = \frac{1}{2\pi} \sum_{m=-\infty}^{\infty} e^{im\theta}. \quad (2)$$

The function $\phi_k(t)$ defines the time structure of the beam passing through the detector. For the moment we will assume that the power in the Schottky signal is independent of this time structure (e.g., the case of a coasting debunched beam). In the next section we will discuss the differences between bunched and debunched beams.

If we consider the $m$th revolution harmonic, $\omega/\omega_0$, the lower betatron sideband is $m - q$, where $q$ is the noninteger part of the betatron tune, and the upper betatron sideband is $m + q$. We denote the revolution frequency of the reference particle as $f_0$ and the single particle revolution frequency as $f_k$.

The signal amplitude near the $m$th revolution harmonic is

$$S_{0,m}(t) = \sum_{k=1}^{N} f_k Q e^{im[\omega_0 t + \phi_k(t)]} \left[ X + \frac{(E_k - E_0)}{\beta^2 E_0} D \right]. \quad (3)$$

With $\omega_\beta = (l + q)\omega_0$, the signal amplitude at the upper betatron sideband is

$$S_{+,m}(t) = \sum_{k=1}^{N} f_k Q e^{i(m-l)[\omega_0 t + \phi_k(t)]} \frac{\hat{X}_k}{2} (e^{i[(l+q)\omega_0 t + \psi_k]}). \quad (4)$$

The power in the signal near the revolution harmonic is proportional to

$$P_0 = \langle |S_{0,m}(t)|^2 \rangle = f_0^2 Q^2 N \left[ X^2 + \frac{\langle (E_k - E_0)^2 \rangle D^2}{(\beta^2 E_0)^2} \right]. \quad (5)$$

The power in the upper ( + ) and lower ( − ) betatron sidebands is proportional to

$$P_+ = P_- = f_0^2 Q^2 N \frac{\langle \hat{X}_k^2 \rangle}{4} = f_0^2 Q^2 N \frac{\sigma^2}{2}. \quad (6)$$

Notice that the power in these spectra is independent of harmonic.

The rms beam size, $\sigma$, is derived by taking the ratio of the power in the $m$th revolution harmonic to the sum of the power in the betatron sidebands:

$$\frac{P_0}{P_+ + P_-} = \frac{1}{\sigma^2} [X^2 + D^2 \delta^2], \quad (7)$$

where

$$\delta^2 = \frac{\langle (E_k - E_0)^2 \rangle}{(\beta^2 E_0)^2}. \quad (8)$$

To measure the rms beam size we scan $X$ and fit the resulting parabola to find $\sigma$ and the dispersion offset.

## V. BUNCHED BEAM ANALYSIS

The primary difference between bunched and debunched beams is that the bunched structure can add power at the revolution harmonic, as a result of bunch structure variations, quadrupole or dipole oscillations, or other coherent phenomena. The result is that a sharp coherent line can appear in the spectrum at the revolution harmonic. In addition, given sufficient resolution bandwidth, the distribution of frequencies in the spectrum will be seen to be broken up into synchrotron sideband components. However, we are interested in the power in the spectrum, which is what we evaluate here.

Consider a single harmonic, $m$, where we now have taken the dispersion to be zero:

$$S_{0,m}(t) = \sum_{k=1}^{N} f_k Q e^{im[\omega_0 t + \phi_k(t)]}(X). \quad (9)$$

For a coasting debunched beam passing through the detector, the time structure is defined by

$$\phi_k(t) = \omega_0 \eta \frac{\Delta p_k}{p} t + \psi_k, \quad (10)$$

where $0 \leq \psi_k < 2\pi$ is the relative particle phase, $\Delta p_k/p$ is the momentum deviation for particle $k$, and $\eta$ is the slip factor equal to $\frac{1}{\gamma_t^2} - \frac{1}{\gamma^2}$.

Since the particles are independently distributed in phase, the individual particle currents cancel and only the rms current remains:

$$\langle |S(t)|^2 \rangle = f_0^2 Q^2 N (X)^2. \quad (11)$$

For a bunched beam with single particle amplitudes $a_k$ and synchrotron frequencies $\Omega_k$, the time structure is defined by

$$\phi_k(t) = a_k \sin(\Omega_k t + \psi_k). \quad (12)$$

The effective signal from all but the revolution harmonic is

$$S_{e,m}(t) = \sum_{k=1}^{N} \sum_{p\neq 0} J_p(ma_k) f_k Q e^{ip(\Omega_k t+\psi_k)}(X), \quad (13)$$

where we have introduced $J_p$, the Bessel function of order $p$,

$$e^{iz\sin\theta} = \sum_{p=-\infty}^{\infty} J_p(z) e^{ip\theta}. \quad (14)$$

In this case, particles arrive only within a short window of time, within which the particle phases are distributed around the synchronous particle according to the potential created by the accelerating voltage in the accelerator. We are only evaluating the power outside of the revolution harmonic. For the observed effective rms signal, only the lowest order Bessel function remains:

$$\langle |S_{e,m}(t)|^2\rangle = \sum_{k=1}^{N} \sum_{p\neq 0} J_p^2(ma_k) f_0^2 Q^2 X^2$$
$$= \sum_{k=1}^{N} [1 - J_0^2(ma_k)] f_0^2 Q^2 X^2. \quad (15)$$

For the moment, assume that the beam has a smooth Gaussian distribution. The rms bunch length, in seconds, for this distribution is $\tau$. As described earlier, the harmonic of the Schottky cavity is $m = \omega/\omega_0$. The bunched beam particle distribution can then be described by

$$\frac{1}{\tau^2}\int_0^\infty x e^{-x^2/2\tau^2} J_p^2(m\omega_0 x) dx = \tau^2 e^{-m^2\omega_0^2\tau^2} I_p(m^2\omega_0^2\tau^2), \quad (16)$$

where $I_p$ is the modified Bessel function of order $p$ of the first kind. Then,

$$\langle |S_{e,m}(t)|^2\rangle = f_0^2 Q^2 X^2 [N - N e^{-m^2\omega_0^2\tau^2} I_0(m^2\omega_0^2\tau^2)]. \quad (17)$$

For large arguments,

$$I_0(x) \approx \frac{1}{\sqrt{2\pi x}} e^x. \quad (18)$$

The power outside the revolution line is then

$$\langle |S_{e,m}(t)|^2\rangle \approx f_0^2 Q^2 X^2 N\left(1 - \frac{1}{\sqrt{2\pi m^2\omega_0^2\tau^2}}\right). \quad (19)$$

If we take the rms bunch length to be 2 nsec and $\frac{m\omega_0}{2\pi} = 2.07$ GHz, then $m\omega_0\tau = 2.07 \times 2\pi \times 2 = 26$. The fraction of power lost when we remove the coherent line from the spectrum is $<1\%$. For the typical bunch lengths in RHIC, the coasting debunched beam approximation is very good. Bunch lengths would have to get extremely short for this approximation not to hold true. Note that this coherent power only occurs at harmonics of the revolution frequency. So no coherent signal resulting from the bunch structure appears in the betatron sidebands.

A general estimate for the Schottky power lost to the revolution line can be found as follows. The quantity of interest is

$$\langle 1 - J_0^2(\omega\tau)\rangle = \int \tau d\tau \rho(\tau)[1 - J_0^2(\omega\tau)] \quad (20)$$

$$\approx \int_0^{\hat{\tau}} \tau d\tau \rho(\tau)\left(1 - \frac{1}{\pi\omega\tau}\right) \quad (21)$$

$$\approx \left(1 - \frac{1}{\pi\omega\hat{\tau}}\right), \quad (22)$$

where we have phase averaged the asymptotic expansion of the Bessel function and defined $\hat{\tau}$ as a "typical" bunch length. For a Gaussian of rms width $\tau$, $\hat{\tau} = (\sqrt{2/\pi})\tau$ while a constant phase space density for $\tau < \tau_0$ gives $\hat{\tau} = \tau_0/2$. From this we conclude that the shape of the longitudinal distribution does not contribute significantly to the power lost to the revolution line, within the range of RHIC parameters.

Other coherent phenomena can contribute to the signal, such as applied transverse signals from other instrumentation. In RHIC, these signals are always kept as small as possible and applied infrequently.

## VI. RHIC HIGH FREQUENCY SCHOTTKY CAVITY

The RHIC high frequency (HF) Schottky cavities are located in a RHIC straight section unoccupied by any experiments, but well beyond the interaction region. There is one cavity for each ring (in RHIC there is a common beam pipe only in the interaction regions). The beam optics parameters at the two cavities are very similar, but can change depending on the configuration of lattice

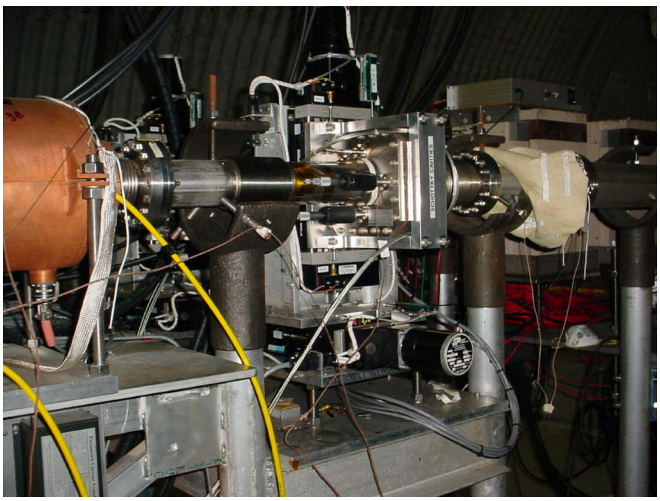

FIG. 1. (Color) High frequency Schottky cavity detector in the RHIC tunnel.

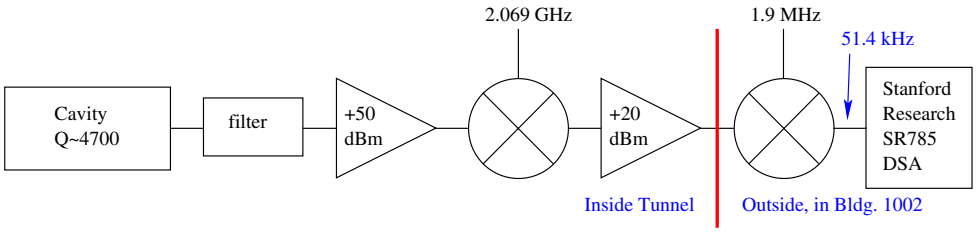


FIG. 2. (Color) Block diagram of the signal processing. The filter, two amplifiers, and the first mixer are located inside the tunnel. The second mixing stage is done in the support building.

optics. Both cavities are movable over a range of about $\pm 25$ mm, in both transverse directions. Figure 1 shows the device in the RHIC tunnel.

With a loaded $Q$ of about 4700 and a center frequency of about 2 GHz, the cavities have a bandwidth of less than 500 kHz. Although they operate at a high frequency, with this high $Q$ the cavity filling time is much longer than the spacing between RHIC bunches. So these devices are not capable of giving bunch by bunch data. Instead they are used to give time averaged results, where the time to process the data is defined by the resolution bandwidth required to get a clean signal above the noise floor.

The signal processing for each cavity consists of a number of stages of amplification and mixing to pull out the small Schottky signals and to bring the frequency of the signal down to a level that we can process it using standard signal processing equipment. The processing of Schottky signals for beam diagnostics is based on what has been learned from the processing of signals for stochastic cooling systems [21–23]. The main difference is stochastic cooling systems are designed to have a much wider bandwidth. For our system very narrow bandpass filtering is performed followed by amplification using low noise, high quality amplifiers. Then a series of signal mixing is performed to bring the frequency down to a level that can be processed in a dynamic analyzer or Fourier transform analyzer. Figure 2 shows a simplified block diagram of the signal processing. The bandpass filter on the output of the cavity is not strictly necessary, but does protect the first amplifier from any lower mode coherent signals that might contain significant power. The bandwidth of the filter is much larger than the frequency response of the cavity at 2.07 GHz, so it does not distort the signal we are processing.

## VII. MEASUREMENTS

We tested this method of measuring the beam size during RHIC run-8 using polarized protons. To measure the power in the three spectral components (the upper and lower betatron sidebands, and the revolution harmonic), we wrote a simple LABVIEW® application to scan the position of the detector, find the peaks of the three components, and measure the power within a narrow range above 3 dBm to the peak. We used a single variable to control how many points in the coherent part of the revolution line to ignore. The same number of points were ignored in each of the betatron sidebands. The power was then taken only from the part of the spectrum from outside of that region to the 3 dBm point. The resulting ratio of the power in the three components was then unaffected by the removal of the coherent line. This method does introduce a systematic error, in that the locations in the three spectral components from which the power was measured might not exactly correspond. The uncertainty introduced by this systematic uncertainty in the power ratio is approximately $\pm 15\%$. Once these parameters were set they remained fixed for an entire scan. The interface for this application is shown in Fig. 3.

A Schottky spectrum for protons during a normal RHIC store is shown in Fig. 4. The central spectral component has a sharp peak in the middle. This is the coherent part of the revolution harmonic. Also shown is the background spectrum with no beam. The background is not flat but is slightly parabolic. The correction for this is small ($\approx 1\%$). Background subtractions were not performed for these measurements but will be included in the future. We also plan to improve the processing of the three components in the spectrum, using fittings and calculating the total power for each line. This will reduce systematic errors that affect the uncertainty in the power ratio calculation.

The results of scanning the position of the two cavities for each transverse plane of the two RHIC rings is shown in Fig. 5. The two rings are distinguished from each other by labeling one the blue ring (beams travel clockwise) and the other the yellow ring (beams travel counterclockwise). For these scans each point represents a 10 pulse average of the power ratio at that detector position. The application automatically moved the detector in predefined steps over a predefined range. The results of the parabolic fits are shown in the figure. From the fitting we obtain $1/\sigma^2$ and $D^2\delta^2$. We also obtain $X_0$, which is the center position of the beam in the detector relative to some arbitrary reference. The value of $X_0$ should be equal to the average beam position as found by the RHIC orbit system plus any offsets in the mechanical positioning of the Schottky cavity. Shown in the figure are the $\chi^2$ for the fits.

In principle, if we derived the momentum spread from the width of the Schottky betatron sidebands, we could also

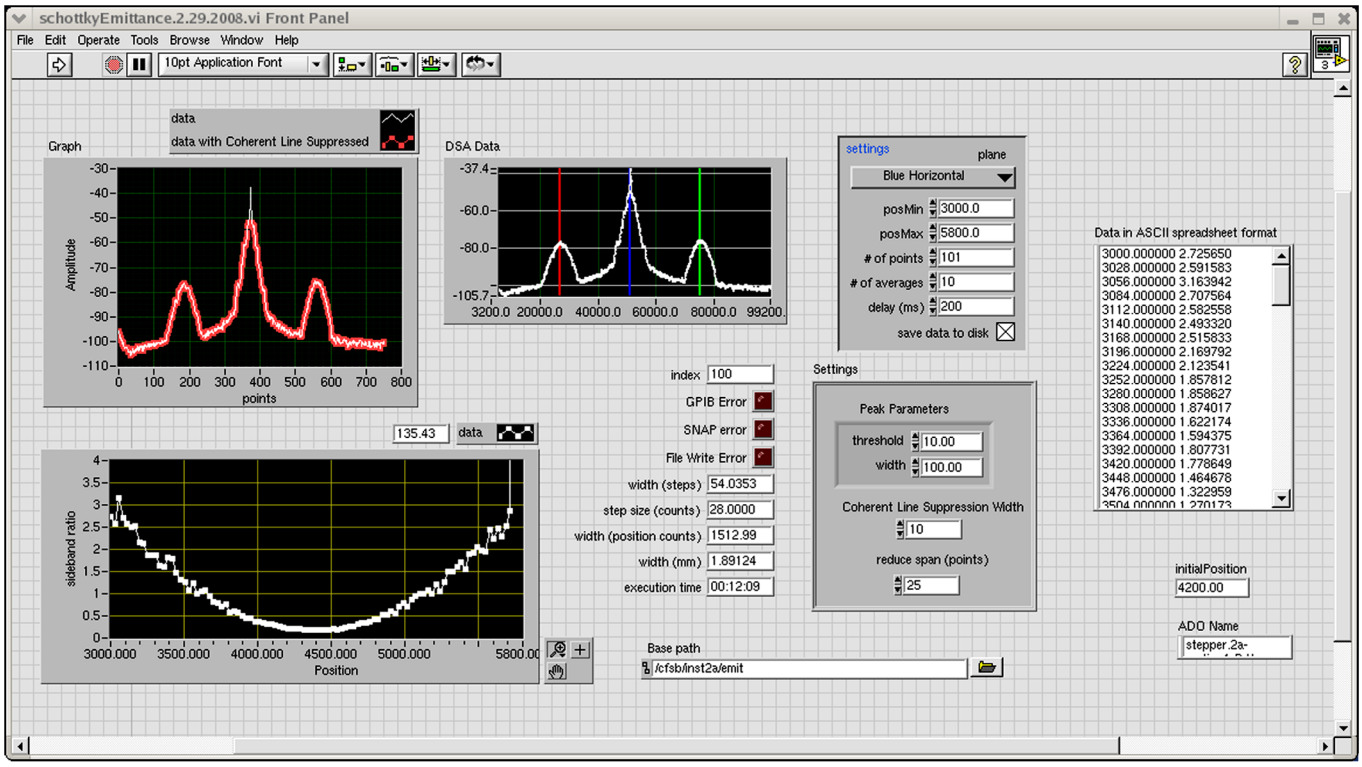


FIG. 3. (Color) LABVIEW® application used to scan the position of the detector and measure the power in the Schottky spectral lines.

obtain the dispersion at the detector. For these measurements we did not extract out the momentum dispersion. We plan to perform further studies to see what precision we can obtain for $D$ and how it compares to orbit measurements of dispersion.

From the one sigma beam size extracted from the fitting we derived beam emittances, using lattice functions from the RHIC online model. Table II summarizes the results and shows a comparison of the emittance derived from the RHIC IPM. Note that the IPM measurements are single sampled data and the Schottky scan is a measure of the average emittance for all RHIC bunches within the time sample of the scan (a few minutes). It is known that there are (mostly) horizontal variations in the position of the beam at the detector, which would cause a slightly larger beam size to be measured. One source of such variations is oscillations in the orbit caused by (mostly 10 Hz) mechanical vibrations of the superconducting low-$\beta$ triplets at the six interaction regions in RHIC [24].

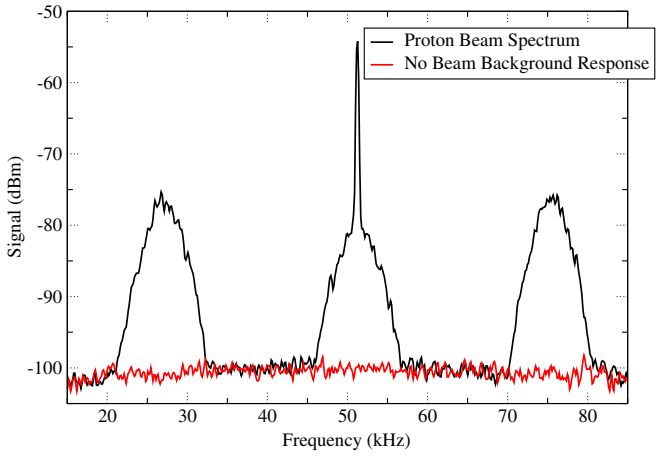


FIG. 4. (Color) A Schottky spectrum and background spectrum taken during normal polarized protons operation.

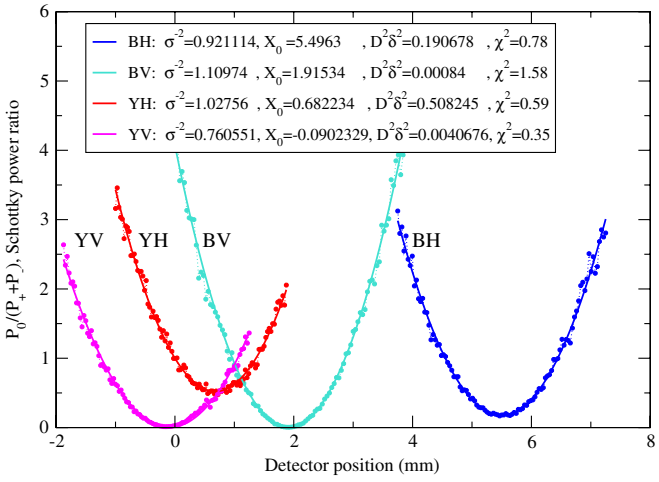


FIG. 5. (Color) Data and fitting results from studies performed during this year's polarized proton run. BH, BV, YH, and YV denote blue ring horizontal, blue ring vertical, yellow ring horizontal, and yellow ring vertical, respectively.

TABLE II. Results of Schottky emittance scan and comparison to RHIC IPM. Emittance values are normalized.

| Ring and plane | Schottky $\beta$ function (m) | Schottky rms beam size (mm) | Schottky emittance ($\pi$ $\mu$m, 95%) | IPM emittance ($\pi$ $\mu$m, 95%) |
|---|---|---|---|---|
| Blue horizontal | $28 \pm 4$ | $1.04 \pm 0.1$ | $23 \pm 5$ | $24 \pm 5$ |
| Blue vertical | $27 \pm 4$ | $0.95 \pm 0.1$ | $20 \pm 4$ | $23 \pm 3$ |
| Yellow horizontal | $27 \pm 4$ | $0.99 \pm 0.1$ | $22 \pm 4$ | $19 \pm 4$ |
| Yellow vertical | $30 \pm 5$ | $1.15 \pm 0.1$ | $26 \pm 5$ | $28 \pm 4$ |

Uncertainties in the calculated emittances given in Table II are largely affected by the uncertainty in the $\beta$ functions at each device. The uncertainties given for the $\beta$ functions are taken from beam based measurements in RHIC. The amount that the $\beta$ functions around RHIC get distorted depends mostly on the set $\beta^*$ at the two experiments (the settings of the low-$\beta$ triplets). Another large factor in the uncertainties is in the uncertainty of the measured beam widths. Evaluation of the uncertainties in the measured widths for the IPM show that the measured scatter in consecutive measurements tend to be around $\pm 3\%$ to $\pm 4\%$. Additional sources of uncertainty (kinematic recoil effects and deterioration or damage to microchannel plates) give the final uncertainty in the range of $\pm 5\%$ to $\pm 10\%$ for the vertical planes and between $\pm 10\%$ to $\pm 15\%$ for the horizontal. Uncertainty due to momentum dispersion is insignificant in comparison to these. After combining these uncertainties with those due to the $\beta$ functions, we find the uncertainty in the IPM measurements can be as large as $\pm 15\%$ for the vertical and $\pm 20\%$ for the horizontal. For the Schottky scans the largest uncertainty is due to the uncertainty in the measured power ratio. The scatter for the 10 point averages in the scans is between $\pm 2\%$ to $\pm 5\%$. After including the systematic uncertainty introduced in the power ratio measurement, the total uncertainty in the Schottky scans we take to be $\pm 20\%$.

## VIII. CONCLUSIONS

The method of scanning the HF Schottky cavity in RHIC to derive the beam size has been developed and tested. Since the method only requires we measure the ratio in the power of the Schottky spectral components, the only calibration required is the calibration in the drive mechanism used to move the cavity. The results agree well within the uncertainties when compared to RHIC IPM measurements. This method will be implemented into normal RHIC operation in future RHIC runs and will enable a nondestructive measurement of beam emittance during physics stores.

## ACKNOWLEDGMENTS

We are very grateful for productive discussions with J. M. Brennan, P. Cameron, R. Connolly, and M. Minty. Technical support for the Schottky systems is provided by J. Cupolo and R. Schroeder. We also thank W. Fischer for providing technical parameters of RHIC. This work was performed under Contract No. DE-AC02-98CH10886 with the auspices of the U.S. Department of Energy.

[1] H. Koziol, CERN internal report, CERN-PS-2001-012-DR, 2001.
[2] A. Drees, B. Fox, Z. Xu, and H. Huang, in *Proceedings of the 20th Particle Accelerator Conference, Portland, OR, 2003* (IEEE, New York, 2003), p. 1688.
[3] A. Drees and Z. Xu, in *Proceedings of the 19th Particle Accelerator Conference, Chicago, Illinois, 2001* (IEEE, Piscataway, NJ, 2001), p. 3120.
[4] S. Van der Meer, CERN internal report, ISR-PO/68-31, 1968.
[5] M. A. Furman and M. S. Zisman, in *Handbook of Accelerator Physics and Engineering* (World Scientific, Singapore, 1999), Chap. 4.1, pp. 247–251.
[6] R. Connolly, R. Michnoff, and S. Tepikian, in *Proceedings of the 21st Particle Accelerator Conference, Knoxville, 2005* (IEEE, Piscataway, NJ, 2005), p. 230.
[7] H. Huang and K. Kurita, AIP Conf. Proc. **868**, 3 (2006).
[8] S. Bellavia, D. M. Gassner, T. Russo, P. Thieberger, D. Trbojevic, and T. Tsang, in Proceedings of the 2007 Particle Accelerator Conference, Albuquerque, New Mexico, 2007 (IEEE, Albuquerque, New Mexico, 2007), p. 2648.
[9] H. Okada *et al.*, AIP Conf. Proc. **980**, 370 (2008).
[10] T. Roser, in Proceedings of the 2007 Asian Particle Accelerator Conference (APAC 07), Indore, India, pp. 74–78.
[11] C. Gardner *et al.*, in *Proceedings of the 11th European Particle Accelerator Conference, Genoa, 2008* (EPS-AG, Genoa, Italy, 2008), p. 2548.
[12] A. Drees *et al.*, in Proceedings of the 2007 Particle Accelerator Conference, Albuquerque, New Mexico, 2007, Ref. [8], p. 722.
[13] C. Montag *et al.*, in Proceedings of the 11th European Particle Accelerator Conference, Genoa, 2008, Ref. [11], p. 2566.
[14] E. D. Courant and H. S. Snyder, Ann. Phys. (Paris) **3**, 1 (1958); **281**, 360 (2000).
[15] Y. Luo *et al.*, in Proceedings of the 2007 Particle Accelerator Conference, Albuquerque, New Mexico, 2007, Ref. [8], p. 4363.

[16] S. van der Meer, *Frontiers of Particle Beams; Observation, Diagnosis and Correction, Diagnostics with Schottky Noise* (Springer, Berlin, 1989), pp. 423–433.
[17] S. Chattopadhyay, CERN SPS/84-11, 1984.
[18] D. Boussard, CERN SPS/86-11 (ARF), 1986.
[19] W. Barry, J. N. Corlett, D. A. Goldberg, and D. Li, in *Proceedings of the 6th European Particle Accelerator Conference, Stockholm, 1998* (IOP, London, 1998), p. 1514.
[20] P. Cameron *et al.*, in *Proceedings of the 5th European Workshop on Beam Diagnostics and Instrumentation for Particle Accelerators, Grenoble, France, 2001* (ESRF, Grenoble, 2001), p. 41.
[21] D. Boussard, S. Chattopadhyay, G. Dôme, and T. Linnecar, CERN internal report, CERN-SPS-84-4-ARF, 1984.
[22] J. P. Marriner and D. McGinnis, AIP Conf. Proc. **249**, 693 (1992).
[23] R. J. Pasquinelli, Nucl. Instrum. Methods Phys. Res., Sect. A **532**, 313 (2004).
[24] C. Montag *et al.*, in Proceedings of the 21st Particle Accelerator Conference, Knoxville, 2005, Ref. [6], p. 3298.